Shear-Induced Melting

Bruce J. Ackerson
Department of Physics, Oklahoma State University, Stillwater, Oklahoma 74078

and

Noel A. Clark
Department of Physics, University of Colorado, Boulder, Colorado 80309

(Received 6 October 1980)

The collective translational structure of dilute suspensions (~ 0.1% by weight) of charged, spherical, and colloidal particles under shear is investigated by light scattering. When subjected to increasing shear rate, the equilibrium bcc Wigner lattice exhibits two major, reversible, disordering transitions. Transition II occurs at low shear, is kink mediated and results in freely slipping two-dimensional hcp layers. At higher rates, transition I occurs where these two-dimensional layers melt via shear-induced fluctuations (phonons) to produce an amorphous structure. The amorphous structure has stringlike particle correlations which ultimately disappear.

PACS numbers: 61.10.-i, 81.30.Fb

In this communication we describe the phenomenology of the shear-induced breakdown of equilibrium crystalline translational order in a qualitatively new regime, where the applied shear is sufficiently large to mechanically melt the crystals. Light scattering is used to probe the effects of shear flow on translational ordering in very dilute colloidal suspensions of highly charged ($Z \sim 10^3$ electron charges), spherical (radius, r = 54.5 or 117 nm), polymer particles in water, interacting via a Coulomb repulsive potential which is screened by H^+ counterions. For sufficiently large concentrations c ($\sim 10^{11}/\mathrm{cm}^3$), such particles will spontaneously order into three-dimensional Wigner crystals,[1,2] which for our experiments were body centered cubic (bcc). These "colloidal crystals" are extremely soft with typical elastic compliances [3] $E \sim 1$ cm^2/dyn; and they have long local structural relaxation times, $\tau_r \sim 10^{-2}$ sec.[4] Because E and τ_r are so large (respective values for typical atomic or molecular crystals are 10^{-9} cm^2/dyn and 10^{-13} sec), colloidal crystals are highly susceptible to distortion and damage by shear stress or flow, and thus can usefully serve as model systems for the study of the response of atomic crystals to conditions of extreme shear.

The suspensions were subjected to shear by two different methods as described previously.[2,4] In one method, a rectangular quartz cell is rocked with frequency ω about an axis normal to its largest faces to provide a local Poiseuille shear profile. The probe laser beam of wave vector $\vec{k}_I$ is directed coincident with the axis of rotation ($\vec{k}_I \perp \hat{v}$), and the intensity distribution $I(\vec{s})$ of the scattered light of (wave vector $\vec{k}_s$) is viewed and photographed on a flat screen normal to the beam and a distance D from the cell. The shear rate is an oscillatory function of time t, but the system disordering dynamics are sufficiently slow that the disordering effects are sensitive only to the time-averaged rms shear rate $S(z) = \langle (\partial v/\partial z)^2 \rangle_t^{1/2}$, which can be controlled by varying ω or the position of the laser beam/rocking axis across the width of the cell face. The second method consists of using a concentric cylinder cell in which the inner cylinder rotates to produce a nearly uniform steady-state shear rate, S, in the contained suspension. Concentric cell data are examined for two scattering geometries $\vec{k}_I \perp \hat{v}, \parallel \hat{\nabla}$ as in rocking cell and $\vec{k}_I \parallel \hat{v}, \perp \hat{\nabla}$. Here the viewing screen is normal to the shear direction, $\hat{\nabla}$, but parallel to the velocity, $\hat{v}$, and third orthogonal direction, $\hat{e}$.

Suspensions were prepared in the cells with a small amount of H-OH ion-exchange resin to gather stray ions. Sphere concentrations were adjusted to allow bcc crystallization at rest. Newly deionized samples exhibited a mosiac of bcc crystallites as evidenced by Bragg-scattering powder patterns. Experiments were carried out at room temperature as the crystals would melt if the temperature T were elevated from 5 to 10 °C.

We now describe the observed increase in order as the shear is decreased. With sufficiently high shear applied, all evidence of crystallization disappears; and the light-scattering pattern consists of diffuse Debye-Scherrer rings [Fig. 1(a)], which are nearly identical to that obtained in the liquid phase[4] (by raising T or lowering c). The first Debye-Scherrer ring with $\vec{k}$-space radius,

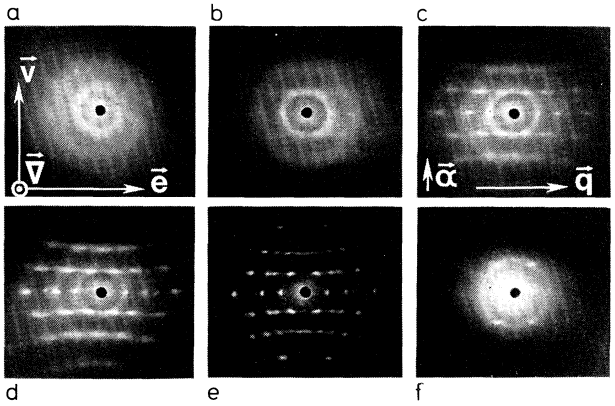

FIG. 1. Scattered-light intensity distributions, $I(\vec{s})$, obtained with use of the rocking cell for $r = 117$ nm [(a) to (e), $D = 47$ nm], and $r = 54.5$ nm radius spheres [(f), $D = 19.4$ mm]. The Ewald sphere (ES) is tangent at $k_\nabla = 0$ to the $\hat{k}_v$-$\hat{k}_e$ plane such that a minor geometrical transformation converts the intensity distribution on the screen, $I(s_v, s_e)$ to the projection of the scattering factor $S(\vec{K})$ onto the $\hat{k}_v$-$\hat{k}_e$ plane. (a) Debye-Scherrer rings of an amorphous, mechanically melted suspension at $S = 17.9$ Hz. (b) $S = 9.3$ Hz. The pre-transition-I region, with diffuse k_v = constant bands and diffuse $k_v = 0$ spots. (c) $S = 8.2$ Hz. Below transition I and above transition II, a 2D hcp in the $\hat{k}_v$-$\hat{k}_e$ plane which is slightly compressed along $\hat{k}_e$ is evident. (d) $S = 4.4$ Hz. Below transition II, an added set of $k_v = 0$ spots appear. (e) $S = 0$. The 3D hcp regions gradually disappear, replaced by either of the two possible bcc structures [see text and Fig. 2(a)]. This shows an intermediate state in this process, which is a superposition of the reciprocal lattices of bcc_1 and bcc_2, smearing them along $\hat{k}_\nabla$, and intersecting them with the Ewald sphere. (f) $S = 6.1$ Hz. Below transition I and above transition II for $r = 54.5$ nm, showing the extinction along $\hat{e}$ of the first-order $k_v = 0$ spots due to the half row displacement of adjacent layers.

$2\pi/a$, was identical to the bcc (110) powder ring radii. Dimensions were $a = 840$ nm for $r = 54.5$ nm, and $a = 2200$ nm for $r = 117$ nm. This "melting" of the original bcc crystal is not a thermal effect as work done on the samples by shear produces changes in T of $< 0.1\,^\circ$C in the worst case. Also, it is reversible in the sense that bcc crystallites begin to reform immediately upon abrupt cessation of shear to make a crystalline powder of random orientation. However, if S is gradually lowered, recrystallization occurs via a series of discrete transitions to structures of partial translational order. These structures are found in both shearing methods by observing the scattered intensity distribution, $I(\vec{s})$.

As the rate of shear is reduced and transition I is approached, diffuse intensity bands appear along lines of constant $k_v = 2n\pi/a$, with $n = \pm 1, \pm 2$, and ± 3, and diffuse spots appear at $k_v = 0$ and $k_e = 2n\pi/a$, with $n = \pm 1$ and ± 2 for the $\vec{k}_I \perp \hat{v}$ geometry [Fig. 1(b)]. Here $2\pi/a$ is the radius of the first Debye-Scherrer ring [Fig. 1(a)]. This $\vec{k}$-space structure indicates the presence of interparticle correlations corresponding to strings of a few particles running parallel to $\hat{v}$, spaced by a mean distance of a along $\hat{e}$ but with no interstring positional correlation along $\hat{v}$.

As S is lowered below transition I, sharp spots appear at $k_v = 0$, $k_e = 2n\pi/b$ and sharp lines appear along $k_v = 2n\pi/a$ for the $\vec{k}_I \perp \hat{v}$ geometry [Fig. 1(c)]. The spots appear at positions which are shifted to smaller $\hat{k}_e$ than the diffuse spots ($b \sim 1.2a$), and are most intense for even orders. Figure 1(f) shows the first-order spots completely absent for the $r = 54.5$ nm suspension in this region. The lines for $k_v = 2n\pi/a$ are modulated in intensity to form rows of spots which are elongated along $\hat{e}$. The resulting pattern in the $\hat{k}_v$-$\hat{k}_e$ plane is a distorted two-dimensional hexagonal close packed (2D hcp) array with a 20% shrinkage along $\hat{e}$. For the $\vec{k}_I \| \hat{v}$ geometry, the Ewald sphere is tangent at $k_v = 0$ to the $\hat{k}_\nabla$-$\hat{k}_e$ plane. At transition I, the amorphous Debye-Scherrer ring, which appears at the position of the zero shear (110) powder pattern ring, transforms to the cross-hatched region shown in Fig. 2(b). The overall $\vec{k}$-space structure is illustrated in Fig. 2(c), where it is seen that the cross-hatched diffuse lines are the intersection with the Ewald sphere of rodlike regions of large $S(\vec{k})$ running parallel to $\hat{k}_\nabla$ and passing through the $\hat{k}_v$-$\hat{k}_e$ plane at 2D hcp (10) spots {the four spots appearing on the central Debye-Scherrer ring at transition I [Fig. 1(c), 1(f)]}. We interpret this $\vec{k}$-space structure as a condensation of the strings into hcp layers which are parallel to the $\hat{e}$-$\hat{v}$ plane and stretched by 20% along $\hat{e}$ [Fig. 2(a)]. Adjacent layers along $\hat{\nabla}$ are displaced parallel to $\hat{e}$ by $b/2$ (half row spacing) which results in a reduction of intensity of odd-order $k_v = 0$ reflections. This $b/2$ displacement and the large interstring spacing are the result of a layer "channeling down the grooves" in the neighboring layers in a shear flow. These sliding 2D hcp layers lack relative translational correlation along $\hat{v}$ which produces the experimentally observed rod structure in $\vec{k}$ space. Also visible in Fig. 1(b) are the diffuse rings which have now become hexagonal. These arise from local hexagonal clusters which are oriented by the shear [Fig. 2(a)], and are apparently distinct

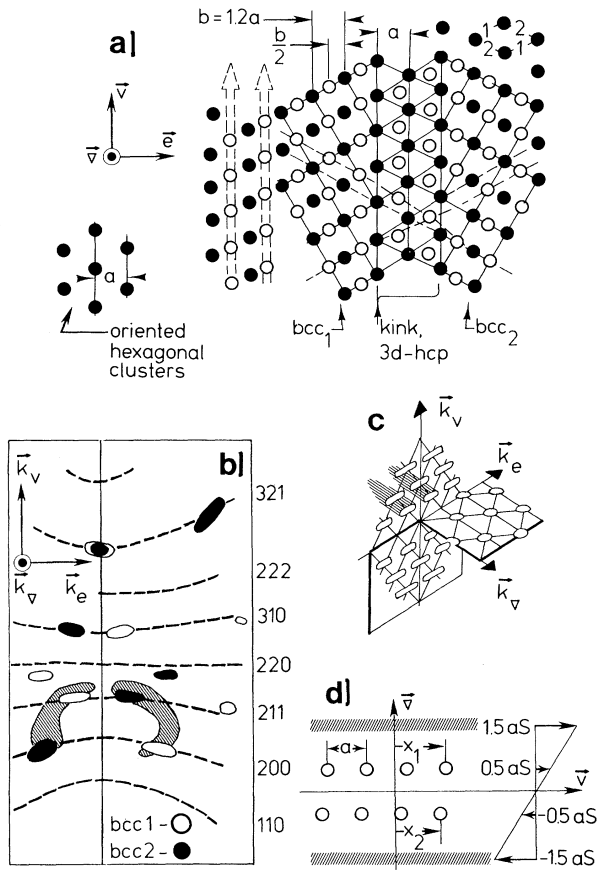

FIG. 2. (a) Schematic of a layer of particles under shear (solid circles) and the adjacent layer (open circles). Above transition I, the layers freely slip along $\hat{v}$ with a $b/2$ relative displacement along $\hat{e}$, as indicated by the dashed arrows. Oriented hexagonal clusters (left) give rise to the hexagonal diffuse rings below transition I [Fig. 1(c)]. Registration sites on lines joining particles to form bcc crystals are indicated by 1 or 2 (upper right). The choice of 1 leads to bcc_1 and similarily for bcc_2. Registration at the centers of three-particle triangles leads to 3D hcp regions which form kinks separating bcc_1 and bcc_2 regions. (b) $I(\vec{s})$ for the rotating cylinder method with $\vec{k}_I \| \hat{v}, \perp \hat{\nabla}$. The Ewald sphere is tangent to the $\hat{k}_\nabla$-$\hat{k}_e$ plane. Cross-hatched diffuse bands appear at transition I and are rods of scattering emanating parallel to $\hat{k}_\nabla$ from the four 2D hcp (10) spots in the $\hat{k}_v$-$\hat{k}_e$ plane. Black and open spots appear below transition II and are assignable to bcc_1 (closed circles) and bcc_2 (open circles) structures, providing evidence for the registration of planes at transition II. (c) Structure of $S(\vec{K})$ between transitions I and II, indicating spots in the $\hat{k}_\nabla$-$\hat{k}_e$ plane, due to the registration of planes along $\hat{e}$; and rods of scattering parallel to $\hat{\nabla}$, a result of the lack of correlation along $\hat{v}$. (d) Two-dimensional system used to model transition II. The effect of layers 0 and 3 on 1 and 2 results in the mean force $\vec{G}$ in the $\hat{v}$ direction.

from the regions ordered into layers as evidenced by the inward displacement of the $k_v = 0$ spots from the diffuse hexagon maximum.

Upon further lowering shear rate, transition II is observed in which the registration of adjacent sheets along $\hat{v}$ is achieved. Because there is a 20% stretch of the 2D hcp sheets along $\hat{e}$, registration sites for adjacent layers lie on the centers of either of two sets of lines joining particles [1 and 2 in Fig. 2(a)] to form locally either of two twin related bcc structures [bcc_1, bcc_2 in Fig. 2(a)], or at the center of triangles formed by three particles to make a local 3D hcp structure [Fig. 2(a)]. Experimentally, transition II is heralded by the appearance of this 3D hcp structure as evidenced by a second set of sharp $k_v = 0$ spots [Fig. 1(d)] which are properly placed to make a $\vec{k}$-space 2D hcp, i.e., at $k_v = 0$ and $k_e = 2n\pi/a$. Registration is further indicated in the $\vec{k}_I \| \hat{v}$ geometry by the disappearance of the diffuse bands and the appearance of a set of discrete spots [Fig. 2(b)]. These are assignable to reciprocal-lattice points of the two bcc crystal orientations. The ultimate structure ($S = 0$) is a mosaic of the two bcc crystal orientations (complete registration with occasional defects). This indicates that the hcp structure must be associated with the state of intermediate S and translational order along $\hat{v}$, a mosiac of bcc_1, bcc_2, and hcp correlated region (a transition region with extensive defects).

Similar features are obtained for closely related one-dimensional model systems represented by a string of harmonically coupled particles subject to a periodic potential, constant applied force, and temperature. Here a transition from binding to free slip mediated by kinks or solitons and occurring at an applied force comparable to the maximum binding force[5-7] is predicted. However, these calculations are not directly applicable for our case because the drag force, $-\vec{\sigma}/\mu \equiv (\dot{\vec{x}} - \vec{v})/\mu$, on a particle is not constant but depends on its velocity $\vec{\sigma}$ relative to the fluid velocity $\vec{v}$, where μ is the mobility of a given particle. Also the time-average particle velocity is necessarily equal to the fluid velocity, $\langle \vec{\sigma} \rangle_t = 0$. Thus, we have modified the above models to describe transition II in a 2D analog of our system, with x_i, the uniform displacements of adjacent layers of particles along $\vec{v}$, obeying a pair of coupled Langevin equations ($i \neq j = 1, 2$):

$$M\ddot{x}_i = -(\dot{x}_i - v)/\mu + G - B \sin[2\pi(x_i - x_j)/a] + f_i(t). \quad (1)$$

Here $aB/2\pi$ is the amplitude of the interrow periodic potential, G is the mean force due to adjacent layers [0 and 3 in Fig. 2(d)] and f_i are fluctuating forces. Requiring $\langle\dot{\phi}\rangle_t \equiv 0$ leads at low temperature to $G = \{[v^2 + (B\mu)^2]^{1/2} - v\}/\mu$ and $\langle\sigma^2\rangle_t = 4\mu G v$, where $\langle\sigma^2\rangle_t$ is a measure of the roughness of the sliding of the rows relative to each other. The transition region corresponds to $v = B\mu$ or a characteristic shear rate $S_c = B\mu/a$, at which G begins to drop and $\langle\sigma^2\rangle_t$ is near maximum. For $B \sim Ea^2 \sim 10^{-8}$ dyn, $\mu = (6\pi\eta r)^{-1} \sim 10^5$ dyn cm/sec, and $a \sim 10^{-4}$ cm, we find $S_c \sim 10$ Hz, in good qualitative agreement with our observations.

A mechanism for transition I is suggested by the structuring of the $k_v > 0$ lines into spots. The spots become more diffuse, especially in the $\hat{k}_e$ direction with increasing $\hat{k}_v$, indicating a broadening arising from transverse lattice vibrations with displacement $\vec{\alpha}$ along $\hat{k}_v$ and wave vector $\vec{q}$ along $\hat{k}_e$ in the 2D hcp sheets as shown in Fig. 2(a). This broadening and hence the 2D lattice vibration amplitude increases with increasing shear rate. As a model for intraplane transverse phonon generation, we considered a layer to be an isotropic elastic membrane subjected to a random thermal force and a drag force due to the local fluid velocity. A displacement in the $\hat{\nabla}$ direction couples to a motion in $\hat{v}$ direction and leads to a larger rms absolute displacement of a point or relative displacement of two points as the shear is increased. The allowed wavelengths in this calculation must be bounded from below by a limit on the number of possible states and from above as well, giving a "size" to the plates within a layer. To satisfy a Lindemann criterion the plates shrink as the shear increases, in agreement with observation. Details of these arguments will be published elsewhere.

One of us (B. J. A.) acknowledges support from the Research Corporation.

[1]R. Williams and R. S. Crandall, Phys. Lett. 48A, 225 (1974).
[2]N. A. Clark, A. J. Hurd, and B. J. Ackerson, Nature 281, 57 (1979).
[3]R. Williams, R. S. Crandall, and P. J. Wojtowicz, Phys. Rev. Lett. 37, 348 (1976).
[4]N. A. Clark and B. J. Ackerson, Phys. Rev. Lett. 44, 1005 (1980).
[5]J. M. Ziman, *Principles of the Theory of Solids*, (Cambridge Univ. Press, Cambridge, 1964), p. 63.
[6]T. Schneider, E. P. Stoll, and R. Morf, Phys. Rev. B 18, 1417 (1978).
[7]S. E. Trullinger, M. D. Miller, R. A. Guyer, A. R. Bishop, F. Palmer, and J. A. Krumhansl, Phys. Rev. Lett. 40, 206, 1603(E) (1978).

Soliton Propagation in ^{3}He-*A*

T. J. Bartolac, C. M. Gould, and H. M. Bozler
Department of Physics, University of Southern California, Los Angeles, California 90007
(Received 12 September 1980)

A propagating magnetic texture has been observed in superfluid ^{3}He-*A* confined to 17-μm slabs with use of pulsed NMR. The results support a model of an expanding lattice of solitons in the order parameter. The propagation velocity approaches the spin-wave velocity as $T \to T_c$, and goes to zero for $T < 0.86T_c$. Despite the narrow geometry, the solitons observed involve distortions of both the spin and orbital degrees of freedom.

PACS numbers: 67.50.Fi, 61.16.Hn, 75.30.Ds

We report the first measurements of a propagating spin-related mode in superfluid ^{3}He-*A*. This work was stimulated by the proposals of Maki and co-workers[1-3] that solitons can exist in the superfluid, and by the successful observation of these metastable textures by several groups.[4-7] Perhaps the most intriguing aspect of solitons is the prediction that they can propagate through the superfluid. We have observed this propagation and find that near T_c the velocity approaches the calculated spin-wave velocity,[8] but decreases at lower temperatures, going to zero for $T/T_c < 0.86$.

The metastable modes in ^{3}He-*A* have been found to be most reliably produced by pulsed transverse NMR, and most easily identified by a change in the NMR frequency. In ^{3}He-*A* this frequency obeys the relation[2,7]

$$\omega^2 = (\gamma H_0)^2 + (R_T \Omega_A)^2, \quad (1)$$

where γH_0 is the Larmor frequency, Ω_A is the longitudinal resonance frequency, and R_T^2 is a constant ($0 \leq R_T^2 \leq 1$) which depends upon the type of texture (soliton) present. We have taken a novel approach to observing the propagation of this

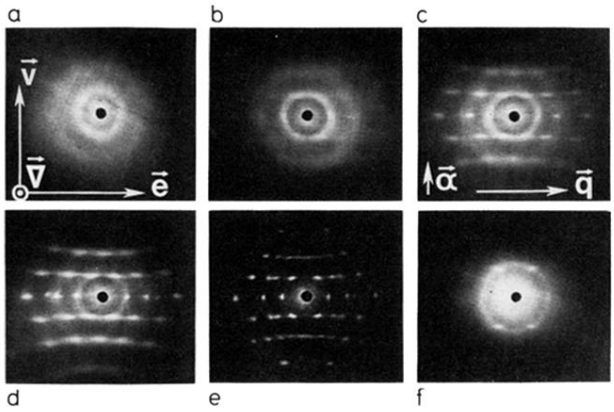

FIG. 1. Scattered-light intensity distributions, $I(\vec{s})$, obtained with use of the rocking cell for $r = 117$ nm [(a) to (e), $D = 47$ nm], and $r = 54.5$ nm radius spheres [(f), $D = 19.4$ mm]. The Ewald sphere (ES) is tangent at $k_{\nabla} = 0$ to the $\hat{k}_v$-$\hat{k}_e$ plane such that a minor geometrical transformation converts the intensity distribution on the screen, $I(s_v, s_e)$ to the projection of the scattering factor $S(\vec{K})$ onto the $\hat{k}_v$-$\hat{k}_e$ plane. (a) Debye-Scherrer rings of an amorphous, mechanically melted suspension at $S = 17.9$ Hz. (b) $S = 9.3$ Hz. The pre-transition-I region, with diffuse k_v = constant bands and diffuse $k_v = 0$ spots. (c) $S = 8.2$ Hz. Below transition I and above transition II, a 2D hcp in the $\hat{k}_v$-$\hat{k}_e$ plane which is slightly compressed along $\hat{k}_e$ is evident. (d) $S = 4.4$ Hz. Below transition II, an added set of $k_v = 0$ spots appear. (e) $S = 0$. The 3D hcp regions gradually disappear, replaced by either of the two possible bcc structures [see text and Fig. 2(a)]. This shows an intermediate state in this process, which is a superposition of the reciprocal lattices of bcc_1 and bcc_2, smearing them along $\hat{k}_{\nabla}$, and intersecting them with the Ewald sphere. (f) $S = 6.1$ Hz. Below transition I and above transition II for $r = 54.5$ nm, showing the extinction along $\hat{e}$ of the first-order $k_v = 0$ spots due to the half row displacement of adjacent layers.